CrystEngComm

Accepted Manuscript

This is an *Accepted Manuscript*, which has been through the Royal Society of Chemistry peer review process and has been accepted for publication.

Accepted Manuscripts are published online shortly after acceptance, before technical editing, formatting and proof reading. Using this free service, authors can make their results available to the community, in citable form, before we publish the edited article. We will replace this *Accepted Manuscript* with the edited and formatted *Advance Article* as soon as it is available.

You can find more information about *Accepted Manuscripts* in the Information for Authors.

Please note that technical editing may introduce minor changes to the text and/or graphics, which may alter content. The journal's standard Terms & Conditions and the Ethical guidelines still apply. In no event shall the Royal Society of Chemistry be held responsible for any errors or omissions in this *Accepted Manuscript* or any consequences arising from the use of any information it contains.

ROYAL SOCIETY OF CHEMISTRY

www.rsc.org/crystengcomm

Please do not adjust margins

CrystEngComm

ARTICLE

The Structure-Dependent Quantum Yield of ZnCdS Nanocrystals

Hong-Shuo Chen,[a] Shu-Ru Chung,[b,*] Ya-Ching Chen,[a] Tsan-Yao Chen,[c] Ching-Yuan Liu[d] and Kuan-Wen Wang[a,*]

Received 00th January 20xx,
Accepted 00th January 20xx

DOI: 10.1039/x0xx00000x
www.rsc.org/

In this study, we demonstrate the effect of atomic arrangement and valence band structures on the optical properties of $Zn_xCd_{1-x}S$ nanocrystals (NCs) by controlling the Zn ratios. Our results indicate that the increases in coordination number of Zn-O bonding within the NCs and structural changes in valence band (VB) would enhance their quantum yield (QY) due to the influence of the surface states and charge recombination rate in VB, respectively. Consequently, the $Zn_xCd_{1-x}S$ NCs with an optimal x =0.4 have the highest QY about 56 %. By combining structural and optical analysis, we systematically elucidate the effect of composition on the local structure and the charge distribution in VB of the $Zn_xCd_{1-x}S$ NCs. Hereby, this study provides mechanistic insight in developing ZnCdS NCs with high QY.

Introduction

Semiconductor nanocrystals (NCs) are one of the most promising candidates for technological applications such as light-emitting devices[1,2], photovoltaic cells[3], bioimaging[4,5] and laser diodes[6,7]. Recently, semiconductor alloy (A_xB_{1-x}) or ternary ($A_xB_{1-x}C$) NCs have attracted much attention because of their unique composition and structure-dependent optical and electronic properties[8-10]. Many studies have shown that some experimental conditions, such as temperatures, ligand types and concentrations, have great influence on the optical properties of NCs[11,12]. Surface ligands are thought to be the most important factors, because when ligands passivize and interact with the precursors, the aggregation states and growth process of NCs can be affected, thus potentially changing their structure and optical properties[13,14]. The effect of surface ligands on the quantum efficiency (QY) of CdTe has been reported [13]. It is noted that both the suitable chain length and the side group are important to control the growth and to improve the optical property of NCs in which the 3-mercaptobutyric acid-modified CdTe NCs exhibit an excellent optical property[13]. Besides, it has been reported that CdTe NCs prepared in trioctylphosphine/dodecylamine are transferred into water. The photoluminescence QY and exciton lifetime are increased accordingly due to the change of band-edge emission[15]. In terms of the CdSe system, the luminescence efficiency has been sufficiently improved by a surface passivation technique[16]. Surfactants can passivate the surface defects which behave as non-radiative relaxation centers for the electron-hole recombination. ZnS or ZnSe and alkylamines are known as typical capping reagents for highly luminescent CdSe NCs[17]. For the ternary NCs, the QYs are affected by the different reaction time and the passivation effects of surface ligands on the NCs surface. Both of the band edge and surface state emission can be tuned by using alkenes of different carbon chain lengths as surface ligands[18].

Moreover, the growth kinetics within NCs including the surface states and growth process, inevitably affects their local structure[19]. For such NCs, lattice strain caused by lattice mismatch, the change in valence band (VB) structure, surface and chemical composition have significant influences on their optical and electronic properties[20-22]. Besides, the lattice strain can also lead to surface or interface trapping and modulate the lattice parameters, which change the intrinsic bond lengths and modify the band structure of the NCs. Although the effect of strain on NCs has been widely studied[23], only few attentions have been paid to understand the influence of VB and local atomic structures on optical properties of ternary NCs, which dictates the overall efficiency in various optoelectronics, photovoltaic and light-emitting applications[24,25].

In this study, highly effective $Zn_xCd_{1-x}S$ NCs with white light emission have been prepared and their composition-dependent lattice strain, VB, and local atomic structure has been discussed. The white light emission comes from single NC instead of a mixture of NC sizes has attracted much attention[26-29] but its mechanism is not yet well established. The white light may be regarded as by chance from surface states or by design from band-edge emissions[26]. The surface-state emission of trap-rich CdS and the dual-color emission from the CdSe core/shell systems show QY of 17 and 30 %, respectively[26]. Moreover, by using aberration-corrected atomic number contrast scanning transmission electron microscopy, it reveals that the white light emitting CdSe NCs are crystalline, consist of approximately four lattice planes,

[a] Institute of Materials Science and Engineering, National Central University, 32001, Taoyuan, Taiwan. Kuanwen.wang@gmail.com.
[b] Department of Materials Science and Engineering, National Formosa University, 63201, Yunlin, Taiwan. srchung@nfu.edu.tw.
[c] Department of Engineering and System Science, National Tsing Hua University, Hsinchu 30013, Taiwan
[d] Department of Chemical and Materials Engineering, National Central University, 32001, Taoyuan, Taiwan.

† Electronic Supplementary Information (ESI) available: XRD, TEM Fourier transformed EXAFS spectra. See DOI: 10.1039/x0xx00000x

CrystEngComm Accepted Manuscript

Please do not adjust margins

and likely have defects[29]. However, there have been few reports regarding the correlation between QY and structural properties of white-light emitting ternary NCs. Therefore, here we have demonstrated the structure-dependent QY of ZnCdS NCs based on the X-ray absorption (XAS) and ultraviolet spectroscopies (UPS). It is observed that the surface oxidation sates, atomic arrangements, QY, and compression strain in NCs can be manipulated by the Zn addition.

Experimental

Preparation of $Zn_xCd_{1-x}S$ NCs

Cadmium oxide (CdO, 99.998 %) was purchased from Alfa Aesar. Zinc oxide (ZnO, 99.999 %), stearic acid (SA, 99 %), sulfur powder (S, 99.98 %), octadecene (ODE, 90 %), hexyldecylamine (HDA, 90 %), and trioctylphosphine oxide (TOPO, 90 %) were obtained by Aldrich. Hexane (99.7 %) and methanol (99 %) were gotten from Mallinckrodt Chemicals. All chemicals were used as received without further purification.

A series of colloidal ternary semiconductor $Zn_xCd_{1-x}S$ (x=0.2, 0.3, 0.4 and 0.5, named as Znx) NCs was prepared by thermal pyrolyzed organometallic route. Total amount of 0.3 mmol of CdO and ZnO were mixed with stearic acid (SA), which served as complex reagents, in a three-necked flask and then heated to 230 ^{o}C under Ar flow until a clear solution was formed to prepare the cadmium/zinc-SA precursor. The solution was then allowed to cool down to room temperature, and a white solid precipitate was obtained. After cadmium/zinc-SA precursor was formed, the mixture solvent, 15 mmol of TOPO and 24 mmol of HDA, was added into three-necked flask and stirred together under Ar at room temperature for 5 min, then reheated the sample up to 320 ^{o}C to form a transparency solution. At this temperature, S-ODE precursor, which was 1.5 mmol of sulfur dissolved in 4 mL of ODE, was swiftly injected into three-neck flask. The nuclei formed quickly and after60 mins, the mixed solution was swiftly cooled down to 150 ^{o}C to stop reaction. Samples were precipitated with hot anhydrous methanol for purification. The precipitate was dissolved in hexane to remove unreacted reagents and excess TOPO or HDA and for further measurement.

Characterization of NCs

The optical properties of samples were measured by Fluorescence Spectrophotometer (FL, Hitachi F-7000) and UV-Visible spectrometer (UV-Vis, Thermo Evolution 60s spectrometer), respectively. Relative QY of samples were determined by comparing the area under the curve of FL emission for the Znx NCs with that of fluorescent dye (Rhodamine 101 in ethanol). Both of sample and reference have the same absorbance under the same absorption wavelength. Phases and structures of NCs were examined by X-ray diffraction (XRD, from Rigaku) with a CuKα (λ=1.54 Å) radiation operated at 40 kV and 25 mA. The XRD patterns were collected by 2θ scan from 20 to 60^{o} with the scan rate of 0.125^{o} per step. Transmission electron microscope (HRTEM, JEOL JEM-2010) was used to analyze the particle size and more than 100 particles were counted to measure the size distribution of samples. The surface chemical states of NCs were conducted by X-ray photoelectron spectroscopy (XPS, Thermo VG Scientific Sigma Probe) using an Al Kα radiation. All binding energies were calibrated with respect to the C 1s line at 284.6 eV. The surface compositions of NCs were estimated by calculating the integral of each peak. The exact chemical compositions of the obtained were measured by inductively coupled plasma – atomic emission spectrometer (ICP-AES, France Horiba JobinYvon JY2000-2) using a standard HCl/HNO_3 digestion. The valence band structure was characterized by photoemission valence band (VB) spectroscopy at beamline of BL24A at National Synchrotron Radiation Research Center (NSRRC) in Taiwan.

The typical XAS spectra of various NCs were obtained in fluorescence mode at the BL01C1 and BL17C1 beamlines at the NSRRC. The incident beam was monochromated using a double crystal monochromator equipped with Si (111) crystal. Si monochromator was employed to adequately select the energy with a resolution ΔE/E better than 1 x 10^{-4} at the Cd K-edge (26711 eV) and Zn K-edge (9659 eV). In general, all NCs were dispersed uniformly on the tape and prepared as thin pellets with an appropriate absorption thickness (μx = 1.0, where μ is the absorption edge and x is the thickness of the sample) so as to attain the proper edge jump step at the absorption edge region. In order to acquire acceptable-quality spectra, each XAS measurement was repeated at least twice and averaged for successive comparison. Moreover, the ionization chamber filled with different mixing gases such as Ar, N_2, He or Kr was used to detect the intensities of the incident beam (I_o), the florescence beam (I_f) and the beam finally transmitted by the reference foil (I_r). For the EXAFS analysis, the backgrounds of pre-edge and post-edge were subtracted and normalized with respect to the edge jump step from the XAS spectra (χ(E)). The normalized χ(E) spectra were transformed from energy to k-space and further weighted by k^3 to distinguish the contributions of back scattering interferences from different coordination shells. Subsequently, the extracted k3-weighted spectra in k-space ranging from 3.0 to 12.9 and 3.3 to 13.0 Å^{-1} for the Cd K-edge and Zn-edge were Fourier transformed into r-space, respectively. The phase correction was set on all spectra in the r-space. Finally, the filtered EXAFS data of Cd K-edge were analyzed by a nonlinear least-squares curve fitting method in the r-space ranging from 1.0 to 3.6 Å^{-1} depending on the bond to be fitted. The reference phase and amplitude for the Cd-O coordination were initially acquired from a CdO powder. Normally, the backscattered amplitude and phase shift functions for specific atom pairs were theoretically estimated by manner of utilizing the FEFF7 code[30]. In addition, the reduction amplitude (S_{02}) value for Cd was fixed at 0.83 in order to determine various structural parameters for each bond pairs.

Results and discussion

The quantum yields (QYs) of various Znx NCs, calculated by comparing the emission area with fluorescent dye (Rodamine 101)[31] are listed in Table 1. The QY is composition-dependent

CrystEngComm Accepted Manuscript

This journal is © The Royal Society of Chemistry 20xx

with the highest value reached to 56 % for Zn0.4. The change of Zn composition may significantly influence the atomic arrangements inside the NCs, thus affecting their optical properties. Fig. 1 shows the emission spectra of Znx NCs, which can be separated into band edge (narrow peak) and trap state (broaden peak) emissions. The band edge emission shifts from 440 to 414 nm with increasing Zn content from 0.2 to 0.5, suggesting the formation of alloyed NCs via the intermixing of the lower band gap CdS (Eg = 2.5 eV) with the higher band gap ZnS (Eg = 3.7 eV)[10,32]. Meanwhile, the other one at longer wavelength with much broad emission band becomes more and more significant with increasing Zn content. It has been reported that in the colloidal InP NCs, when the surface sates are passivated, the NCs show only band-edge emission with very high QY[33]. Previously, we have also observed that the surface state emission plays an important role in enhancing the QY.[34] Therefore, the quantitative integral emission area results of Znx NCs are summarized in Table 1 in order to investigate the QY enhancement factor. It seems that the area ratio of surface state to total emissions ($A_s/(A_s+A_b)$) increases as the Zn content increases, suggesting that either the Zn content or the atomic arrangement can influence the optical properties of the NCs[35]. Moreover, the insert in Fig. 1 compares the quantitative emission areas of NCs. The result implies that this absolute emission area including the surface states and band edges determines the QY, especially for Zn0.4. It is worth mentioning that the emission area dramatically drops for Zn0.5, maybe attributed to the structure-dependent effect.

The phases and structures of the Znx NCs characterized by XRD are displayed in Fig 2. The corresponding structural parameters are summarized in Table S1 in supporting information (SI). Clearly, the various Znx NCs possess the face center cubic (FCC) CdS crystallites, and the diffraction peaks located at 26.46, 43.89 and 51.98° correspond to the characteristic signals from (111), (220) and (311) facets, respectively. For Znx NCs with x = 0.2, 0.3, and 0.4, the upshift of diffraction peaks is mainly caused by the heteroatomic intermix of Zn atoms to CdS crystallite with lattice strain in CdS domains. On the contrary, when Zn composition is increased from 0.4 to 0.5, the diffraction peak position downshifts to lower angle region, suggesting that the main phase is changed from CdS to ZnS, which is also further verified by the results of ICP and XPS later. It is noted that in ZnS dominate system (Zn0.5) the QY of NCs is lower than that in CdS system (Zn0.4)[36,37]. Besides, the lattice strain of ZnCdS (S_{ZnCdS}) NCs is determined by the extent of their characteristic peaks offset from the peak of CdS crystals, with the careful background subtraction as estimated by equation 1:

$$(S_{ZnCdS}) = \frac{a_{ZnCdS} - a_{ref(CdS)}}{a_{ref(CdS)}} \times 100\ \% \quad (1)$$

where a_{ZnCdS} and $a_{ref(CdS)}$ is the lattice constant of the bulk CdS and obtained Znx NC, respectively. As listed in Table 1, this lattice strain is enhanced when Zn content is increased from 0.2 to 0.4, in which the Zn0.4 NCs have the compression as high as 3.60 %, probably promoting its QY.

The morphologies of the Znx NCs are displayed in Fig. 3 and their lattice structural parameters are summarized in Table S2. The Zn_x NCs with a spherical shape have an average particle size of 3.6±0.4, 3.1±0.4, 3.1±0.3 and 2.7±0.4 nm and the interplanar spacing is 3.36, 3.29, 3.15 and 3.32 for Zn0.2, Zn0.3, Zn0.4 and Zn0.5, respectively, As indicated, the interplanar spacing of Znx NCs, are all smaller than that of FCC CdS (3.37 Å), suggesting the lattice compression in Znx NCs as compared in Table 1. Moreover, besides the lattice strain, the atomic arrangement and electronic structures can be manipulated by controlling the Zn addition. On the other hand, in order to understand the exact surface and chemical composition of NCs, XPS and ICP-AES were used and the results are shown in Table 1. The surface Zn/Cd composition of Zn0.2, Zn0.3, Zn0.4 and Zn0.5 is 88/22, 87/13, 42/58 and 79/21, respectively. It is interesting to mention that the surface composition of Zn in Zn0.4 NCs is much higher than the chemical composition which measured by ICP (65/35), indicating that the structure of Zn0.4 NCs is Zn-rich on the outer shell and Cd rich in the inner core. This core/shell structure significantly different from other samples may be one of the QY enhancement factor. Fig. 4 displays the Zn and Cd XANES spectra of Znx NCs, in which the electronic structures, including the oxidation state and site symmetry of the absorbing atom can be clarified. The absorption peak at 9656 eV in Fig. 4 (a) corresponds to the electronic transitions of Zn 1s to 4p states, and the peak at 26711 eV in Fig. 4 (b) is ascribed to the transitions of Cd 1s to 5p states[38]. Herein, the white-line (WL) intensity is an indication for the oxidation level of Zn and Cd atoms, which can be caused by the charge donation from Zn and Cd to their neighbouring atoms. On the other hand, the energy shift of the WL in Zn and Cd K-edge is believed to relate with the change in the bond lengths of Znx NCs at different Zn compositions[15]. The XAS determined corresponding Fourier transformed radial structure function (RSF) profiles and fitting structural parameters of Zn K-edge are provided in Fig. S1(a) and summarized in Table S2 in SI, respectively. For $Zn_{0.2}$, the radial peaks at ~1.95, 2.29 and 3.08 Å are related to the interferences of photoelectrons by Zn-O, Zn-S and Zn-Zn bond pairs, and their coordination numbers are determined to be 2.1, 0.4 and 0.3, respectively. Besides, the calculated degree of oxidation (i.e. N_{ZnO} and N_{CdO}) shown in Table 1 of all samples indicates that the coordination of Zn-O of the NCs can be well-improved after incorporation of Zn from Zn0.2 to Zn0.4, thus promoting the QY. As compared in Table 1, this surface reconstruction is optimized for Zn0.4, resulting in the largest lattice strain within the NCs. In the case of Cd-K edge, the peak located at ~2.20 and ~2.50 Å can be assigned to the contribution of interference from the Cd-O and Cd-S bond pairs, respectively. It is interesting to mention that the atomic arrangement in the Cd pairs has the opposite trend to that in Zn pairs. For Zn0.4 with the highest N_{ZnO} in Zn edge has the lowest N_{CdO} in Cd edge, suggesting an extremely Cd core and Zn shell structure with a very large compression.

The proposed valence charge transition induced by the lattice strain is further investigated by the VB photoemission spectroscopy. Fig 5 compares the VB spectra of various Znx

CrystEngComm Accepted Manuscript

NCs. The charge distribution area near the VB interface of Zn0.4 is much higher than that of other samples, resulting in the high charge recombination rate of NCs. Moreover, it can be seen that when the composition of Zn is increased to 0.5, the charge distribution is decreased significantly, also affecting the QY.

Conclusions

In summary, we demonstrate the correlation between atomic/VB structure and QY of ZnCdS NCs. Our optical analyses elucidate that QY of Zn0.4 as high as 56 % is owing to the largest absolute emission area in FL among all NCs. Moreover, based on the XAS characterization, Zn0.4 NCs possess the Zn shell/Cd core structure with the highest and lowest degree of Zn and Cd oxidation, respectively. In the view point of bulk analysis, this Zn0.4 NCs have the CdS phase while for Zn0.5, the main phase changes to ZnS. This Zn addition from 0.4 to 0.5 results in not only the decrease of lattice strain but also the core/shell inversion, resulting in the decay of QY. The Zn addition would manipulate the QY through control of the surface oxidation sates, atomic arrangements, and compression strain in NCs.

Acknowledgements

This work was supported by the Ministry of Science and Technology of Taiwan under Contract no. 103-2221-E-008-039 and 103-2120-M-007-005. . The authors would like to thank the staff of National Synchrotron Radiation Research Center (NSRRC), Hsinchu, Taiwan for the help in various synchrotron-based measurements techniques

Notes and references

1 V. L. Colvin. M. C. Schlamp and A. P. Alivisatos. *Nature*, 1994, **370**, 354.
2 V. I. Klimov, S. A. Ivanov, J. Nanda, M. Achermann, I. Bezel, J. A. McGuire and A. Piryatinski. *Nature*, 2007, **447**, 441.
3 N. C. Greenham, X. Peng and A. P. Alivisatos. *Phys. Rev. B*, 1996, **54**, 17628.
4 M. Jr. Bruchez, M. Moronne, P. Gin, S. Weiss and A. P. Alivisatos. *Science*, 1998, **281**, 2013.
5 W. C. W. Chan and S. Nie. *Science*, 1998, **281**, 2016.
6 V. I. Klimov, A. A. Mikhailovsky, S. Xu , A. Malko , J. A. Hollingsworth , C. A. Leatherdale , H. J. Eisler and M. G. Bawendi. *Science*, 2000, **290**, 314.
7 H. J. Eisler, V. C. Sundar, M. G. Bawendi, M. Walsh, H. I. Smith and V. Klimov. *Appl. Phys. Lett.*, 2002, **80**, 4614.
8 R. E. Bailey and S. M. Nie. *J. Am. Chem. Soc.*, 2003, **125**, 7100.
9 X. H. Zhong, M. Y. Han, Z. L. Dong, T. J. White and W. Knoll. *J. Am. Chem. Soc.*, 2003, **125**, 8589.
10 X. H. Zhong, Y. Y. Feng, W. Knoll and M. Y. Han, *J. Am. Chem. Soc.*, 2003, **125**, 13559.
11 V. Lesnyak, N. Gaponik and A. Eychmuller, *Chem. Soc. Rev.*, 2013, **42**, 2905.
12 A. L. Rogach, T. Franzl, T. A. Klar, J. Feldmann, N. Gaponik, V. Lesnyak, A. Shavel, A. Eychmuller, Y. P. Rakovich and J. F. Donegan, *J. Phys. Chem. C*, 2007, **111**, 14628.
13 T. Fang, K. Ma, L. Ma, J. Bai, X. Li, H. Song and H. Guo, *J. Phys. Chem. C*, 2012, **116**, 12346.
14 G. L. Wang, Y. M. Dong and Z. J. Li, *Nanotechnology*, 2011, **22**, 085503.
15 S. F. Wuister, I. Swart, F. van Driel, S. G. Hickey and C. D. Donega, *Nano Lett.*, 2003, **3**, 503.
16 T. Trindade, P. O'Brien and N. L. Pickett, *Chem. Mater.*, 2001, **13**, 3843.
17 M. A. Hines and P. Guyot-Sionnest, *J. Phys. Chem. B*, 1998, **102**, 3655.
18 Y. C. Chen, H. S. Chen, S. R. Chung, J. K. Chang and K. W. Wang, *J. Mater. Chem. C*, 2015, DOI: 10.1039/C5TC00903K.
19 J. Y. Rempel, M. G. Bawendi and K. F. Jensen, *J. Am. Chem. Soc.*, 2009, **131**, 4479.
20 A. M. Smith and S. Nie. *Acc. Chem. Res.*, 2010, **43**, 190.
21 A. M. Smith, A. M. Mohs and S. Nie. *Nature Nanotech*., 2009, **4**, 56.
22 G. Ouyang, W. G. Zhu, C. Q. Sun, Z. M. Zhu and S. Z. Liao. *Phys. Chem. Chem. Phys.*, 2010, **12**, 1543.
23 A. I. Persson, M. T. Bjork, S. Jeppesen, J. B. Wagner, L. R. Wallenberg and L. Samuelson. *Nano Lett.*, 2006, **6**, 403.
24 D. N. Talwar, Z. C. Feng, J. F. Lee and P. Becla. *Phys. Rev. B*, 2013, **87**, 165208.
25 D. W. Ayele, H. M. Chen, W. N. Su, C. J. Pan, L. Y. Chen, H. L. Chou, J. H. Cheng, B. J. Hwang and J. F. Lee. *Chem. Eur. J.*, 2011, **17**, 5737.
26 S. Sapra, S. Mayilo, T. A. Klar, A. L. Rogach and J. Feldmann, *Adv. Mater.*, 2007, **19**, 569.
27 M. J. Bowers II, J. R. McBride and S. J. Rosenthal, *J. Am. Chem. Soc.*, 2005, **127**, 15378.
28 A. D. Dukes III, M. A. Schreuder, J. A. Sammons, J. R. McBride, N. J. Smith and S. J. Rosenthal, *J. Chem. Phys.*, 2008, **129**, 121102.
29 M. J. Bowers II, J. R. McBride, M. D. Garrett, J. A. Sammons, A. D. Dukes, M. A. Schreuder, T. L. Watt, A. R. Lupini, S. J. Pennycook and S. J. Rosenthal, *J. Am. Chem. Soc.*, 2009, **131**, 5730.
30 S. I. Zabinsky, J. J. Rehr, A. Ankudinov, R. C. Albers and M. J. Eller. *Phys. Rev. B*, 1995, **52** 2995.
31 T. Karstens and K. Kobs, *J. Phys. Chem.*, 1980, **84**, 1871.
32 B. A. Korgel and H. G. Monbouquette, *Langmuir*, 2000, ***16***, 3588.
33 O. I. Micic, J. Sprague, Z. Lu and A. J. Nozik. *Appl. Phys. Lett.*, 1996, **68**, 3150.
34 H. S. Chen, S. R. Chung, T. Y. Chen and K. W. Wang. *J. Mater. Chem. C*, 2014, **2**, 2664.
35 L. Y. Chen, P. A. Yang, C. H. Tseng, B. J. Hwang and C. H. Chen, *Appl. Phys. Lett.*, 2012, **100**, 163113.
36 Jie Mao, Jun-Na Yao, Li-Na Wang, Wei-Sheng Liu. *J. Colloid Interface Sci.* 2008, **319**, 353.
37 H. Li, W. Y. Shih and W. H. Shih. *Nanotechnology*, 2007, **18**, 205604.
38 W. Zheng, Y. L. Wu, Y. T. Chen, Z. C. Feng , J. F. Lee , P. Becla and R. S. Zheng. *Adv. Mater. Res.*, 2013, **706**, 56.

CrystEngComm Accepted Manuscript

This journal is © The Royal Society of Chemistry 20xx

Table 1. The optical, chemical and structural parameters of Zn_x NCs

NCs	Quantum Yield (%)	$A_S/(A_S+A_B)$[a]	S_{ZnCdS}[b] (%)	Surface /Chemical Compositions[c] Cd:Zn	N_{ZnO}[d] (%)	N_{CdO}[d] (%)
Zn0.2	26	0.37	-1.54	88:12/78:22	0.75	0.29
Zn0.3	42	0.49	-3.08	87:13/67:33	0.80	0.24
Zn0.4	56	0.59	-3.60	42:58/65:35	0.84	0.18
Zn0.5	27	0.65	-2.74	79:21/51:49	0.64	0.34

[a] A_S: Surface state emission area, A_B: Band edge emission area
[b] S_{ZnCdS} : lattice strain of Zn_x NCs
[c] Surface and chemical compositions measured by XPS and ICP.
[d] Degree of oxidation (N_{ZnO}: $CN_{Zn\text{-}O}/CN_{Total}$ and N_{CdO}: $CN_{Cd\text{-}O}/CN_{Total}$)

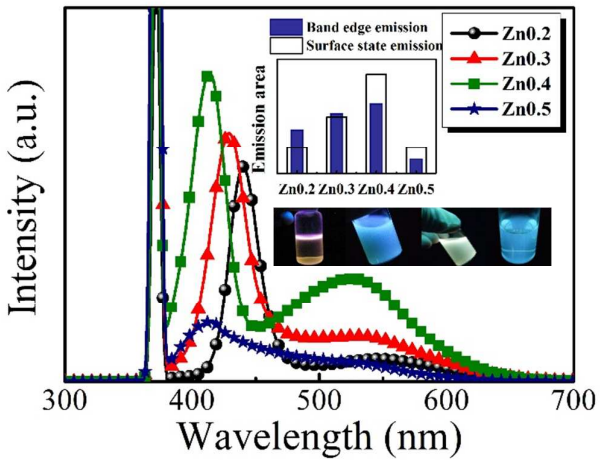

Fig. 1 The emission spectra and luminescent images of Znx NCs. Inset shows the emission area of NCs.

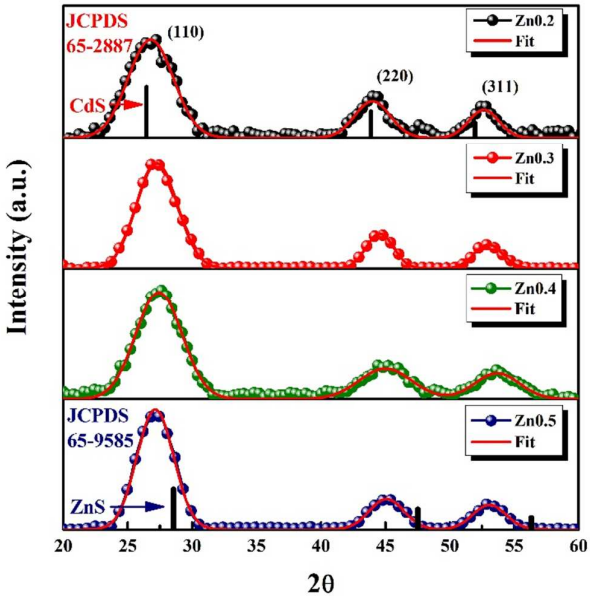

Fig. 2 XRD patterns with fitting curves of various Znx NCs.

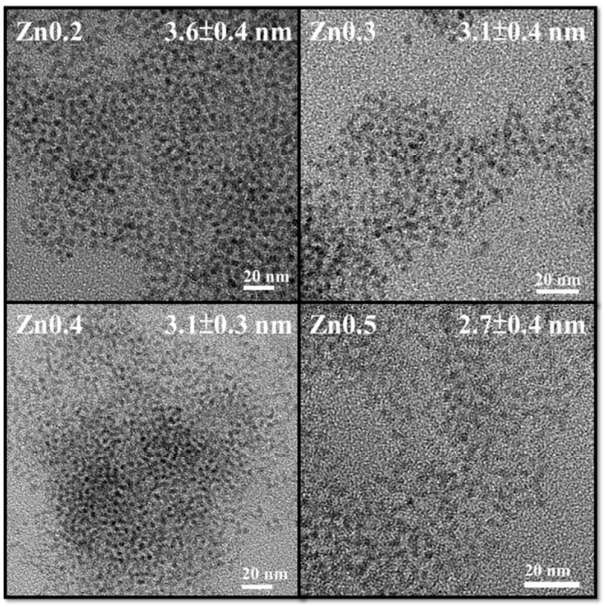

Fig. 3 TEM images of Znx NCs.

CrystEngComm Accepted Manuscript

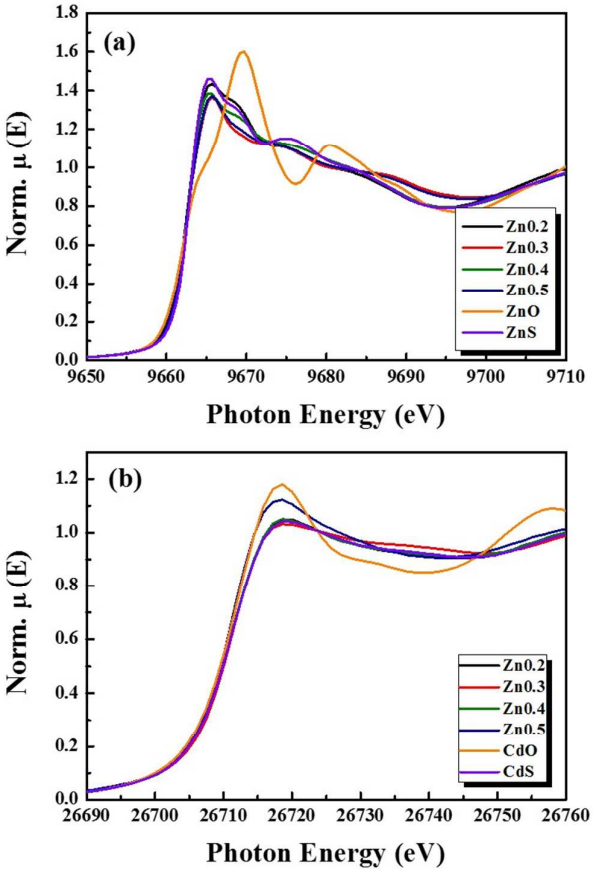

Fig. 4 XANES spectra of Znx NCs at (a) Zn K-edge and (b) Cd K-edge.

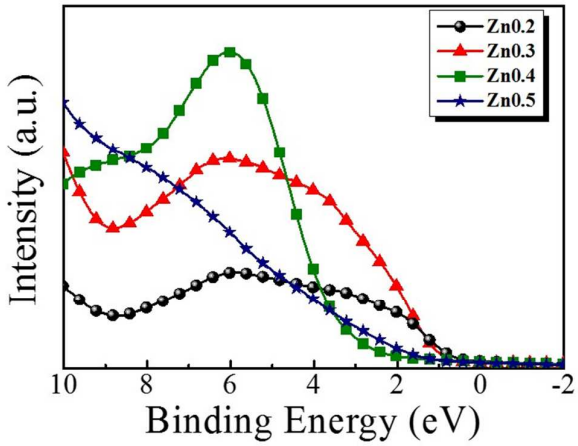

Fig. 5 The valence band spectra of the Znx NCs.

CrystEngComm Accepted Manuscript

This journal is © The Royal Society of Chemistry 20xx

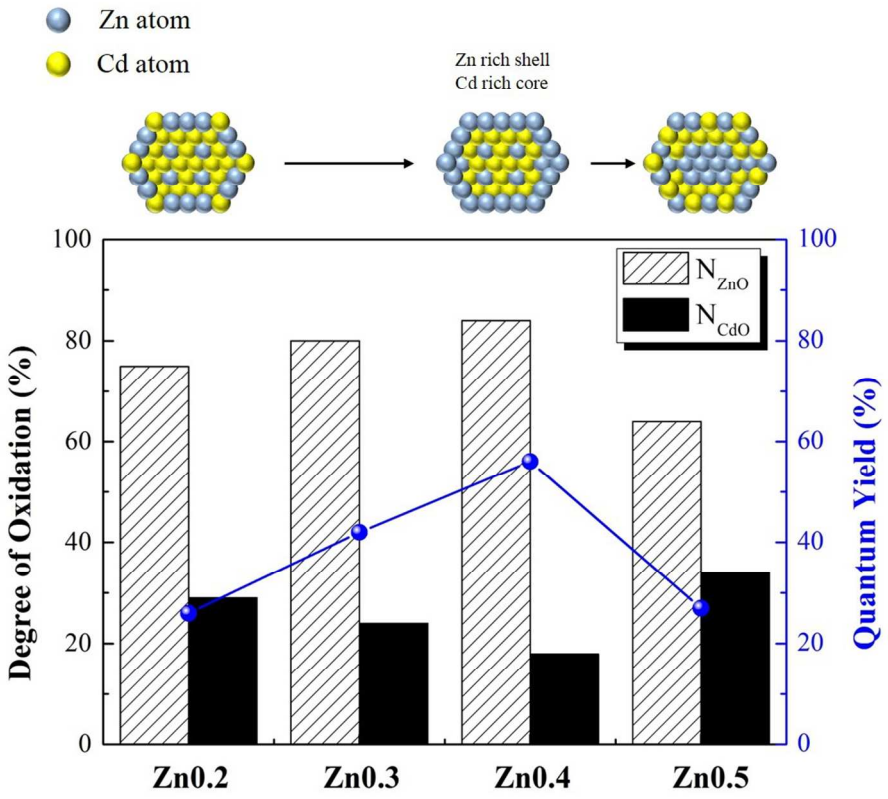

206x179mm (150 x 150 DPI)

CrystEngComm Accepted Manuscript